

The Dynamic Sensorium competition for predicting large-scale mouse visual cortex activity from videos

Polina Turishcheva^{1,*}, Paul G. Fahey^{2-6,*}, Michaela Vystrčilová¹, Laura Hansel¹, Rachel Froebe²⁻⁶, Kayla Ponder^{2,3}, Yongrong Qiu^{1,4-6}, Konstantin F. Willeke^{1,4-8}, Mohammad Bashiri^{1,7,8}, Eric Wang^{2,3}, Zhiwei Ding^{2,3}, Andreas S. Tolias^{2-6,9*}, Fabian H. Sinz^{1,2,3,7,8,*}, and Alexander S. Ecker^{1,10,*}

¹Institute of Computer Science and Campus Institute Data Science, University of Göttingen, Germany

²Department of Neuroscience, Baylor College of Medicine, Houston, TX, USA

³Center for Neuroscience and Artificial Intelligence, Baylor College of Medicine, Houston, TX, USA

⁴Department of Ophthalmology, Byers Eye Institute, Stanford University School of Medicine, Stanford, CA, US

⁵Stanford Bio-X, Stanford University, Stanford, CA, US

⁶Wu Tsai Neurosciences Institute, Stanford University, Stanford, CA, US

⁷International Max Planck Research School for Intelligent Systems, University of Tübingen, Germany

⁸Institute for Bioinformatics and Medical Informatics, University of Tübingen, Germany

⁹Department of Electrical Engineering, Stanford University, Stanford, CA, US

¹⁰Max Planck Institute for Dynamics and Self-Organization, Göttingen, Germany

*Equal contributions

arXiv:2305.19654v2 [q-bio.NC] 12 Jul 2024

Understanding how biological visual systems process information is challenging due to the complex nonlinear relationship between neuronal responses and high-dimensional visual input. Artificial neural networks have already improved our understanding of this system by allowing computational neuroscientists to create predictive models and bridge biological and machine vision. During the Sensorium 2022 competition, we introduced benchmarks for vision models with static input (i.e. images). However, animals operate and excel in dynamic environments, making it crucial to study and understand how the brain functions under these conditions. Moreover, many biological theories, such as predictive coding, suggest that previous input is crucial for current input processing. Currently, there is no standardized benchmark to identify state-of-the-art dynamic models of the mouse visual system. To address this gap, we propose the Sensorium 2023 Benchmark Competition with dynamic input (<https://www.sensorium-competition.net/>). This competition includes the collection of a new large-scale dataset from the primary visual cortex of ten mice, containing responses from over 78,000 neurons to over 2 hours of dynamic stimuli per neuron. Participants in the main benchmark track will compete to identify the best predictive models of neuronal responses for dynamic input (i.e. video). We will also host a bonus track in which submission performance will be evaluated on out-of-domain input, using withheld neuronal responses to dynamic input stimuli whose statistics differ from the training set. Both tracks will offer behavioral data along with video stimuli. As before, we will provide code, tutorials, and strong pre-trained baseline models to encourage participation. We hope this competition will continue to strengthen the accompanying Sensorium benchmarks collection as a standard tool to measure progress in large-scale neural system identification models of the entire mouse visual hierarchy and beyond.

Keywords. mouse visual cortex, system identification, neural prediction, dynamic stimulus

Introduction

Understanding how the visual system processes visual information has been a longstanding goal of neuroscience. Neural system identification, the development of accurate predictive models of neural population activity in response to arbitrary input, is a powerful approach to develop our understanding on a quantitative, testable, and reproducible basis. Systems neuroscience has used a variety of modeling approaches to study the visual cortex in the past, including linear-nonlinear (LN) models (Heeger, 1992a,b; Jones & Palmer, 1987; Simoncelli et al., 2004), energy models (Adelson & Bergen, 1985), subunit models (Liu et al., 2017; Rust et al., 2005; Touryan et al., 2005; Vintch et al., 2015), Bayesian models (George & Hawkins, 2005; Walker et al., 2020), redundancy reduction models (Perrone & Liston, 2015), and predictive coding models (Marques et al., 2018). Deep learning has significantly advanced the performance of predictive models, particularly with the introduction of convolutional neural networks (CNNs) trained on image recognition tasks (Cadena et al., 2019; Cadieu et al., 2014; Yamins et al., 2014) or trained end-to-end on predicting neural responses (Antolik et al., 2016; Bashiri et al., 2021; Batty et al., 2017; Burg et al., 2021; Cadena et al., 2019; Cowley & Pillow, 2020; Ding et al., 2023b; Ecker et al., 2018; Franke et al., 2022; Fu et al., 2023; Kindel et al., 2019; Klindt et al., 2017; Lurz et al., 2021; McIntosh et al., 2016; Sinz et al., 2018; Walker et al., 2019; Wang et al., 2023; Zhang et al., 2018). More recently, transformer-based architectures have also shown strong performance in predicting neural responses (Li et al., 2023).

In some cases, predictive models may be engineered with specific constraints in order to draw insight from interpretable internal parameters. On the other hand, even

Correspondence: turishcheva@cs.uni-goettingen.de; pgfahey@stanford.edu; ecker@cs.uni-goettingen.de

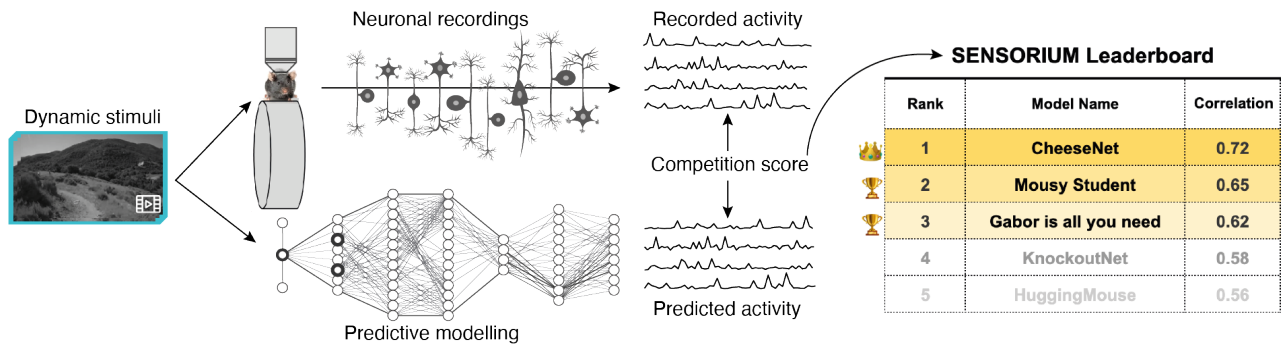


Fig. 1. A schematic illustration of the SENSORIUM competition. We will provide large-scale datasets of neuronal activity in the primary visual cortex of mice. Participants of the competition will train models on pairs of natural image stimuli and recorded neuronal activity, in search for the best neural predictive model.

“black-box” models can still provide important scientific utility. For example, high-performing, data-driven models allow unbiased exploration of large stimulus spaces *in silico* that would otherwise be prohibitively costly with biological experiments, yielding novel insights about the visual system that are evaluated by selective verification by systems neuroscientists *in vivo* (Bashivan et al., 2019; Ding et al., 2023b; Franke et al., 2022; Fu et al., 2023; Hoefling et al., 2022; Ponce et al., 2019; Ustyuzhaninov et al., 2022; Walker et al., 2019; Wang et al., 2023). Additionally, another research focus could be to develop models that generalize well from the training domain (e.g. natural movies) to novel out-of-domain stimuli (Ren & Bashivan, 2023). Such models can also dramatically extend the variety of questions that can be asked of the same dataset by characterizing classical vision tuning properties (e.g. orientation tuning and receptive field location) or novel hypothesis-driven tuning that may be costly or impossible to characterize *in vivo* (Ding et al., 2023a,b; Fu et al., 2023; Wang et al., 2023). Thus, improving predictive performance of these models opens up new avenues for important neuroscientific inquiry.

Standardized large-scale benchmarks are one important approach to steadily accumulate improvements in predictive models, through constructive competition between models compared on equal ground (Dean et al., 2018). Several neuroscience benchmarks already exist, including *Brain-Score* (Schrimpf et al., 2018, 2020), *Neural Latents ’21* (Pei et al., 2021), *Algonauts* (Cichy et al., 2021, 2019; Gifford et al., 2023) and *Sensorium 2022* (Willeke et al., 2022). There are also several recent large datasets that have been released as high-throughput recording methodologies become more available, including the MICrONS calcium imaging dataset (MICrONS Consortium et al., 2021) and calcium imaging and Neuropixel datasets from the Allen Brain Observatory (de Vries et al., 2020; Siegle et al., 2021) However, these large public datasets typically lack the private test set and benchmark infrastructure for third party evaluation of performance metrics on withheld test data.

Importantly, the majority of the above models, competitions, and datasets focus on predicting responses to static stimuli, typically with relatively long presentation times (i.e. hundreds of milliseconds). While this approach has yielded

important insights into the spatial preferences of neural populations, understanding how visual neurons process spatiotemporal information is crucial, because real-life visual stimuli are dynamic. Animals need to be able to accurately and quickly detect and respond to external elements in their environment (e.g. when tracking prey or avoiding a predator), as well as correctly estimate their own motion. Thus, further developing and assessing the performance of models designed for neural predictions over time (Batty et al., 2017; McIntosh et al., 2016; Sinz et al., 2018; Wang et al., 2023; Zheng et al., 2021) is important. However, the field currently lacks a large-scale benchmark for models predicting single-cell responses to dynamic (movie) stimuli.

To address this gap, we propose the *SENSORIUM 2023* competition, aimed at fostering the development of more accurate predictive dynamic models of the mouse visual cortex. These predictive dynamic models take as input video stimuli and/or behavioral variables, and as output predict video-rate responses of single neurons (Fig. 1). We designed and collected a large-scale dataset for this competition, including ten scans from the primary visual cortex of ten mice. In total, the dataset contains responses from 78,853 neurons to a diverse set of videos from various domains, along with behavioral measurements (Fig. 2). The main track will focus on predicting neuronal activity in response to natural videos, with participants encouraged to use behavioral data to enhance their predictions. To test how well the models generalize, a bonus track will evaluate model performance on five out-of-domain stimuli not included in the training set, including parametric stimuli that have been used to characterize classical visual tuning properties. We also provide a starting kit to lower the barrier for entry, with tutorials, code for training baseline models, and APIs for data loading and submission. This competition is part of an ongoing series of *SENSORIUM* competitions for benchmarking predictive models of neuronal responses with the hope that it facilitates our understanding of the computations carried out by visual sensory neurons.

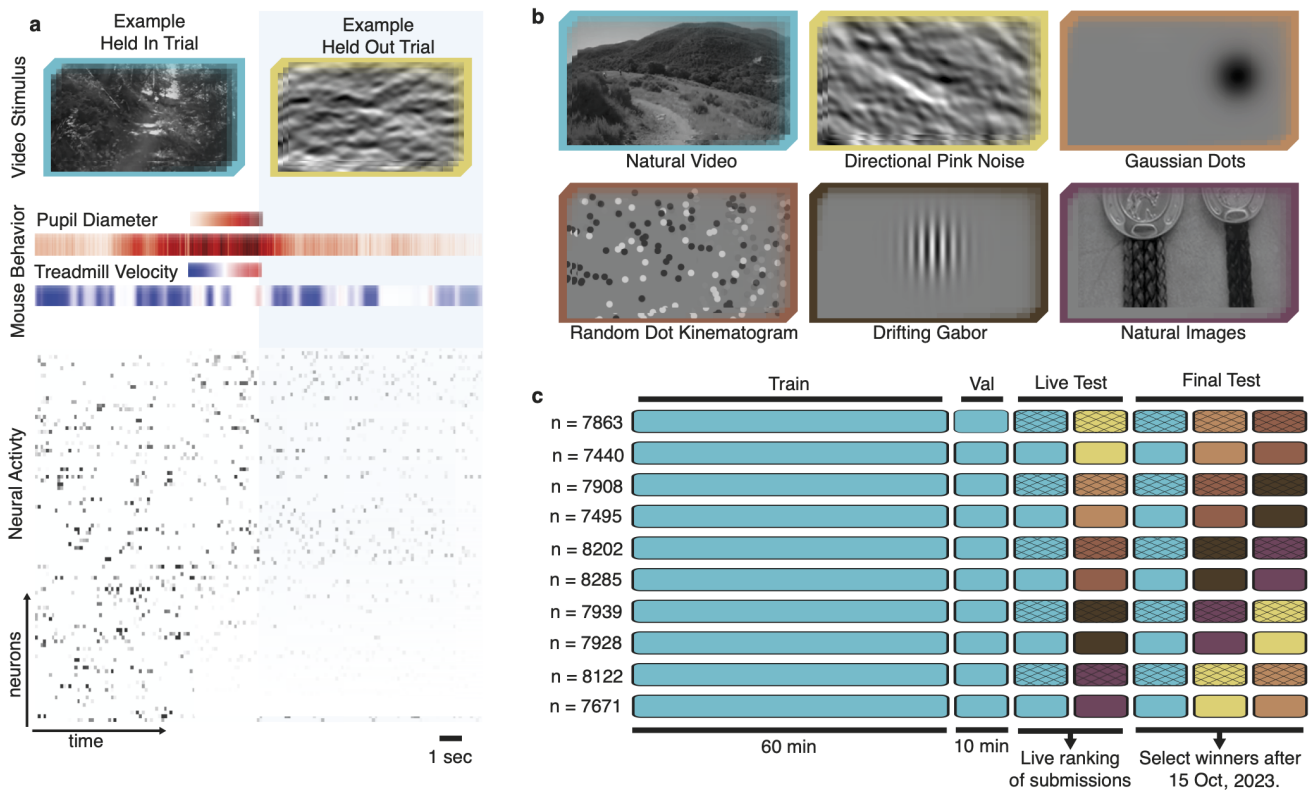


Fig. 2. Overview of the data. **a**, Example stimulus frames, behavior (pupil position not depicted) and neural activity. **b**, Representative frames from natural video and five OOD stimuli. **c**, Stimulus composition (color) and availability for ten animals. The crossed elements were used for live and final test sets in the competition evaluation. For non-crossed elements all responses are available. n is number of neurons per scan.

SENSORIUM competition overview

The goal of the SENSORIUM 2023 competition is to identify accurate predictive dynamic models of mouse visual cortex. Participants are provided with training data in the form of videos that were shown to the mouse, and the resulting recorded neuronal responses and behavioral variables, all of which were recorded for this purpose and will be made public for the first time as part of the competition¹. Participants are then tasked with creating models that predict a test set of withheld neuronal responses from the corresponding video stimuli and behavioral variables. Submissions to the main track are evaluated on a test set of natural video stimuli of the same type present in the training set (i.e. in-domain performance). Submissions to the bonus track are evaluated on a test set of stimulus types not present in the training set (i.e., out-of-domain performance), including static natural images, random dot kinematograms, drifting gabors, gaussian dots, and directional pink noise, as in Wang et al. (2023). For the neurons evaluated as a part of the competition no OOD responses are provided. The test set trials are divided into two exclusive groups: *live* and *final test*. Performance metrics computed on the *live test* trials will be used to maintain a public leaderboard throughout the submission period, while the performance metrics on the *final test* trials will be used to identify the

winning entries, and will only be revealed after the submission period has ended (Fig. 2d). By separating the *live test* and *final test* set performance metrics, we are able to provide feedback from the *live test* set to participants wishing to submit updated predictions over the course of the competition (up to one submission per day), while avoiding overfitting for the *final test* set over multiple submissions. In both cases, the withheld competition test set responses will not be (and have never been) publicly released.

To make the competition accessible for both computational neuroscientists and machine learning practitioners, we will release a *starting kit* that contains the complete code to fit our baseline models as well as explore the full dataset.²

Data

We recorded data with the goal of comparing models that predict neuronal activity in response to dynamic movies. We also include behavioral variables in our dataset as a common proxy of modulatory effects of neuronal responses (Niell & Stryker, 2010; Reimer et al., 2014). Thus, in generic terms, neural predictive models capture neural responses $\mathbf{r} \in \mathbb{R}^{n \times t}$ of n neurons for t timepoints as a function $\mathbf{f}_\theta(\mathbf{x}, \mathbf{b})$ of both natural movie stimuli $\mathbf{x} \in \mathbb{R}^{w \times h \times t}$, where w and h are video width and height, and behavioral variables $\mathbf{b} \in \mathbb{R}^{k \times t}$, where k is the types of behavior ($k = 4$, see

¹<http://sensorium-competition.net/>

²https://github.com/ecker-lab/sensorium_2023/

below). In the following paragraphs, we provide a short description of each one of these quantities.

Movie stimuli. We sampled natural dynamic stimuli from cinematic movies and the Sports-1M dataset (Karpathy et al., 2014), as described in (MICrONS Consortium et al., 2021). Five additional out of domain (OOD) stimulus types, including natural images from ImageNet (Russakovsky et al., 2015; Walker et al., 2019), flashing Gaussian dots, random dot kinematograms (Morrone et al., 2000), directional pink noise (MICrONS Consortium et al., 2021), and drifting Gabors (Petkov & Subramanian, 2007) were also included in the stimulus, in line with earlier work (Wang et al., 2023). Stimuli were converted to grayscale and presented to mice in $\sim 8 - 11$ second clips at 30 Hz (Fig. 2b).

Neuronal responses. Using a wide-field two-photon microscope (Sofroniew et al., 2016), we recorded the responses of excitatory neurons at 8 Hz in layers 2–5 of the right primary visual cortex in awake, head-fixed, behaving mice using calcium imaging. Neuronal activity was extracted as described previously (Wang et al., 2023) and resampled at 30 Hz to be at the same frame rate as the visual stimuli (Fig. 2a). We will also release the anatomical coordinates of the recorded neurons.

Behavioral variables. We provide measurements of four behavioral variables: locomotion speed, which is recorded from a cylindrical treadmill at 100 Hz and resampled to 30 Hz, and pupil size, horizontal and vertical pupil center position, which are extracted from tracked eye camera video at 20 Hz and resampled to 30 Hz.

Dataset. Our complete corpus of data comprises ten recordings in ten animals, which in total contain the neuronal activity of 78,853 neurons to a total of ~ 1200 minutes of dynamic stimuli over the dataset, with ~ 120 minutes per recording (Fig. 2c). None of the ten recordings have been published before, and were released as part of this competition explicitly for this purpose. Five were released on the first day of the competition, but accidentally included responses for live and final test sets, and were thus released in their entirety as pretraining data. An additional five scans were collected for competition evaluation, and were added to the release with live and final test set data withheld.

Each animal recording consists of 4 components (Fig. 2c):

- **Training set:** 60 minutes of natural movies, one repeat each (60 minutes total).
- **Validation set:** 1 minute of natural movies, ten repeats each (10 minutes total).
- **Live test set:** 1 minute of natural movies and 1 minute of OOD stimuli, ten repeats each (20 minutes total). Each OOD stimulus type is represented once in the live test set across the five recordings.
- **Final test set:** 1 minute of natural movies and 2 minutes of OOD stimuli, ten repeats each (30 minutes total). Each OOD stimulus type is represented twice in the final test set across the five recordings.

For the first five mice the responses for all components are released, while for the mice used for competition evaluation only train and validation responses are available publicly. For the training set and validation set, the stimulus frames, neuronal responses, and behavioral variables are released for model training and evaluation by the participants, and are not included in the competition performance metrics. Please note that train and validation sets for the mice used for evaluation only contain natural movies and not the OOD stimuli.

Data availability. The complete corpus of data is available for download¹. To decrease the requirement for local storage, the competition dataset is available through Deep Lake (Hambardzumyan et al., 2022) in a convenient format for use with standard model-fitting techniques, allowing caching data subsets for training.

Baseline models

SENSORIUM 2023 is accompanied by three model baselines (table 1):

- **GRU baseline** is a dynamic model with a 2D CNN core and gated recurrent unit (GRU) inspired by earlier work (Sinz et al., 2018), but replacing the factorized readouts with more recently developed Gaussian readouts as in (Lurz et al., 2021). Conceptually, the 2D core transforms each frame of the video visual stimulus into a latent space, and the GRU persists certain elements from this latent space through time. The Gaussian readout learns the spatial preference of each neuron in visual space (“receptive field”), the position at which a vector from the latent space is extracted. This latent vector is convolved by a vector of weights learned per neuron (“embedding”) to predict the activity of the neuron at a specified time point.
- **Factorized baseline** is a dynamic model with a 3D factorized convolution core and Gaussian readouts inspired by earlier work (Hoefling et al., 2022). In contrast with the GRU baseline, where the 2D CNN core does not interact with the temporal component, the factorized core learns both spatial and temporal components at each layer. This allows the model to transform both spatial and temporal components iteratively as the dimensionality of the latent space changes with increasing channels across layers.
- **Ensembled baseline** is simply an ensembled version of the above factorized baseline over 14 models. Ensembling is a well-known tool to improve the model performance in benchmark competitions (Allen-Zhu & Li, 2023). In order to focus the results of the competition on novel architectures and training methods beyond simple ensembling, only entries outperforming the ensembled baseline will be candidates for competition winners.

Competition Evaluation

Similar to SENSORIUM 2022, for each submission we will compute and report two metrics:

¹<http://sensorium-competition.net/>

Competition track		Baseline performance on held out test data			
		Live test set		Final test set	
		Single Trial Correlation	Correlation to Average	Single Trial Correlation	Correlation to Average
Main Track	Ensembled Baseline	.206	.381	.197	.371
	3D Factorized Baseline	.177	.337	.164	.321
	GRU Baseline	.108	.207	.106	.207
Bonus Track	Ensembled Baseline	.128	.234	.129	.241
	3D Factorized Baseline	.112	.204	.121	.223
	GRU Baseline	.061	.106	.059	.106

Table 1. Performance of the baseline models on both competition tracks. Three baseline scores are provided for each competition track. The minimum performance for winning entries is indicated in bold.

- **Single-trial correlation** on the natural video final test set will be used to determine competition winners for the main track. We will also compute the single-trial correlation metric for each of the five OOD stimulus test sets separately, and the mean single-trial correlation across all five OOD final test sets will be used to determine the competition winner for the bonus track.
- **Correlation to average** is also calculated for research purposes. This metric is more robust to noise due to averaging ground truth data over repeats, but it does not measure how well a model accounts for stimulus-independent variability caused by behavioral fluctuations. For all metrics, the first 50 frames of the prediction and neuronal responses will be discarded before computing. This is to allow a “burn-in” period for dynamic models that rely on history to reach maximum performance. For more details and equations, please see Methods.

Discussion

Here, we introduced the *SENSORIUM 2023* competition for finding the best predictive model for neuronal responses in mouse primary visual cortex to dynamic stimuli. This competition is the second in a series, and shares much of its structure with preceding year’s competition, *SENSORIUM 2022*. Similar to last year, we have included a starting kit with baseline model tutorials, in order to continue supporting accessibility for both neuroscientists and machine learning experts interested in participating. We also once again collected a dedicated large-scale dataset, including an estimated 246% increase in unique neuron-hours above the preceding year. Importantly, we made several major changes in this iteration, including moving from static to dynamic stimuli, adding out-of-domain performance in the bonus track, and including behavior in both tracks. These changes pose new technical challenges and broaden the variety of scientific questions to work on.

The *SENSORIUM 2023* challenge differs from existing benchmarks in that it is the only benchmark for predicting single-cell responses to dynamic natural movie stimuli. The *Brain-Score* benchmark (Schrimpf et al., 2018, 2020) recently added a dynamic component, asking models to predict the temporal evolution of neural activity, but it still

focuses on static images as stimuli. In addition, its scientific goal is not to benchmark predictive models, but to evaluate how well task-pretrained computer vision models match the neural representations along the primate ventral stream. The *Neural Latents Benchmark ’21* (Pei et al., 2021) tests models of neural population activity, but focuses on dimensionality reduction and extracting a small set of latent variables from high-dimensional neural population activity, not necessarily in response to visual stimuli. The *Algonauts challenge* is similar in spirit to last year’s *SENSORIUM 2022* and focuses on predictive models in response to natural images (Cichy et al., 2019; Gifford et al., 2023) or natural video (Cichy et al., 2021), but tests models of functional magnetic resonance imaging (fMRI) in human visual cortex, as opposed to single-cell responses in mouse as in *SENSORIUM*.

This competition also departs from *SENSORIUM 2022* in that both tracks now include behavioral measurements as model inputs. One key issue in assessing model performance is the fact that neural responses are noisy – repeated presentation of the same stimulus does not produce identical responses. This question has been addressed by numerous authors, but no clear consensus has emerged (Haefner & Cumming, 2008; Hsu et al., 2004; Pasupathy & Connor, 2001; Roddey et al., 2000; Schoppe et al., 2016). The usual solution is to attempt to estimate the trial-to-trial variability through the use of repeated stimulus presentations, and then estimate a noise-corrected version of the explained variance (See Pospisil & Bair, 2020, for an in-depth discussion and evaluation of existing metrics as well as a proposal of an asymptotically unbiased estimator). However, not everything determining neural responses is under experimental control. For example, the freely varying behavioral state of the animal modulates neuronal responses, and by including behavioral variables as predictors we can increase the model predictive performance. Yet in consequence, we lose the ability to estimate the “noise” level, because every trial is now a unique combination of behavior and stimulus. As a result, there is no way to determine the maximum achievable performance of a model without additional assumptions, and thus existing approaches for addressing unexplainable trial-to-trial fluctuations are not applicable. For this reason we opted to use the simplest

possible measure of performance: the correlation coefficient between model prediction and observed response on a single-trial basis. While this metric serves our primary purpose of comparing models, it lacks the desirable property of assigning a perfect model a correlation of 1. Whether and how it is possible to obtain performance estimates with non-vacuous upper bounds once behavioral variables are included as model predictors is an open research question for future work.

We plan to continue running the family of *SENSORIUM* competitions with regular dataset releases and challenges, which will persist as benchmarks once the competition has ended. Our hope is these competitions and datasets are not only a technical resource, but also a basis for community formation around developing and testing models. We expect that encouraging discussion around predictive modeling between machine learning practitioners and computational neuroscientists will create opportunities to exchange ideas and benefit from each other's expertise.

Acknowledgments

FHS is supported by the Carl-Zeiss-Stiftung and acknowledges the support of the DFG Cluster of Excellence "Machine Learning – New Perspectives for Science", EXC 2064/1, project number 390727645 as well as the German Federal Ministry of Education and Research (BMBF) via the Collaborative Research in Computational Neuroscience (CRCNS) (FKZ 01GQ2107). This work was supported by an AWS Machine Learning research award to FHS. MB and KW were supported by the International Max Planck Research School for Intelligent Systems. This project has received funding from the European Research Council (ERC) under the European Union's Horizon Europe research and innovation programme (Grant agreement No. 101041669). The project received funding by the Deutsche Forschungsgemeinschaft (DFG, German Research Foundation) via Project-ID 454648639 (SFB 1528), Project-ID 432680300 (SFB 1456) and Project-ID 276693517 (SFB 1233).

This research was supported by National Institutes of Health (NIH) via National Eye Institute (NEI) grant RO1-EY026927, NEI grant T32-EY002520, National Institute of Mental Health (NIMH) and National Institute of Neurological Disorders and Stroke (NINDS) grant U19-MH114830, NINDS grant U01-NS113294, and NIMH grants RF1-MH126883 and RF1-MH130416. This research was also supported by National Science Foundation (NSF) NeuroNex grant 1707400. The content is solely the responsibility of the authors and does not necessarily represent the official views of the NIH, NEI, NIMH, NINDS, or NSF.

This research was also supported by the Intelligence Advanced Research Projects Activity (IARPA) via Department of Interior/Interior Business Center (DoI/IBC) contract no. D16PC00003, and with funding from the Defense Advanced Research Projects Agency (DARPA), Contract No. N66001-19-C-4020. The US Government is authorized to reproduce and distribute reprints for governmental purposes notwithstanding any copyright annotation thereon. The views and

conclusions contained herein are those of the authors and should not be interpreted as necessarily representing the official policies or endorsements, either expressed or implied, of IARPA, DoI/IBC, DARPA, or the US Government.

AUTHOR CONTRIBUTIONS

PT: Conceptualization, Formal Analysis, Investigation, Methodology, Project Administration, Software, Data Curation, Validation, Visualization, Writing - Original Draft, Writing - Review and Editing **PGF:** Conceptualization, Data Curation, Methodology, Formal Analysis, Investigation, Methodology, Project Administration, Software, Validation, Visualization, Writing - Original Draft, Writing - Review and Editing **LH:** Software, Writing - Original Draft, Writing - Review and Editing **RF:** Investigation, Data Curation **KP:** Investigation **MV:** Software **KFW:** Conceptualization, Methodology **MB:** Data Curation **EW:** Conceptualization, Methodology **ZD:** Investigation **AST:** Conceptualization, Methodology, Funding Acquisition, Supervision, Writing - Review and Editing **FHS:** Conceptualization, Methodology, Funding Acquisition, Supervision, Writing - Review and Editing **ASE:** Conceptualization, Methodology, Funding Acquisition, Supervision, Writing - Review and Editing

Materials and Methods

Neurophysiological experiments. All procedures were approved by the Institutional Animal Care and Use Committee of Baylor College of Medicine. Ten mice (*Mus musculus*, 4 females, 6 males, P78–146 on day of first scan) expressing GCaMP6s in excitatory neurons via *Slc17a7-Cre* and *Ai162* transgenic lines (recommended and generously shared by Hongkui Zeng at Allen Institute for Brain Science; JAX stock 023527 and 031562, respectively) were anesthetized and a 4 mm craniotomy was made over the visual cortex of the right hemisphere as described previously (Froudarakis et al., 2014; Reimer et al., 2014).

Mice were head-mounted above a cylindrical treadmill and calcium imaging was performed using Chameleon Ti-Sapphire laser (Coherent) tuned to 920 nm and a large field of view mesoscope (Sofroniew et al., 2016) equipped with a custom objective (excitation NA 0.6, collection NA 1.0, 21 mm focal length). Laser power after the objective was increased exponentially as a function of depth from the surface according to:

$$P = P_0 \times e^{(z/L_z)} \quad (1)$$

Here P is the laser power used at target depth z , P_0 is the power used at the surface (not exceeding 21 mW), and L_z is the depth constant (220 μm). The greatest laser output of 94 mW was used at approximately 425 μm from the surface, with most scans not requiring more than 80 mW at similar depths.

The craniotomy window was leveled with regards to the objective with six degrees of freedom. Pixel-wise responses from an ROI spanning the cortical window (3600 \times 4000 μm , 0.2 px/ μm , approx. 200 μm from surface, 2.47 Hz) to drifting bar stimuli were used to generate a sign map for delineating visual areas (Garrett et al., 2014). Area boundaries on the sign map were manually annotated. Our target imaging site was a 630 \times 630 μm ROI within the boundaries of primary visual cortex (VISp, Supp. Fig. 1).

The released scans contained 10 planes, with 25 μm interplane distance in depth, and were collected at 7.98 Hz. Each plane is 630 \times 630 μm (252 \times 252 pixels, 0.4 px/ μm). The most superficial plane in each volume was approximately 200 μm from the surface. This 25 μm sampling in z

was designed to reduce the number of redundant masks arising from multiple adjacent planes intersecting with the footprint of a single neuron.

Movie of the animal's eye and face was captured throughout the experiment. A hot mirror (Thorlabs FM02) positioned between the animal's left eye and the stimulus monitor was used to reflect an IR image onto a camera (Genie Nano C1920M, Teledyne Dalsa) without obscuring the visual stimulus. The position of the mirror and camera were manually calibrated per session and focused on the pupil. Field of view was manually cropped for each session to contain the left eye in its entirety, ranging from 214–308 pixels height \times 250–331 pixels width at ca. 20 Hz. Frame times were time stamped in the behavioral clock for alignment to the stimulus and scan frame times. Video was compressed using Labview's MJPEG codec with quality constant of 600 and stored in an AVI file.

Light diffusing from the laser during scanning through the pupil was used to capture pupil diameter and eye movements. A DeepLabCut model (Mathis et al., 2018) was trained as previously described (Willeke et al., 2022) on 17 manually labeled samples from 11 animals to label each frame of the compressed eye video (intraframe only H.264 compression, CRF:17) with 8 eyelid points and 8 pupil points at cardinal and intercardinal positions. Pupil points with likelihood >0.9 (all 8 in 55–99% of frames) were fit with the smallest enclosing circle, and the radius and center of this circle was extracted. Frames with < 3 pupil points with likelihood >0.9 ($<0.9\%$ frames per scan), or producing a circle fit with outlier > 5.5 standard deviations from the mean in any of the three parameters (center x, center y, radius, $<0.3\%$ frames per scan) were discarded (total $<0.9\%$ frames per scan). Gaps in behavior were replaced by linear interpolations over the whole session, if there were more than 2 frames with gaps, then the video is removed. (We removed $\sim 2\%$ of the videos, 155 out of 7280, where one video was rejected due to signal synchronization issues during resampling).

The mouse was head-restrained during imaging but could walk on a treadmill. Rostro-caudal treadmill movement was measured using a rotary optical encoder (AccuCoder 15T-01SF-2000NV1ROC-F03-S1) with a resolution of 8000 pulses per revolution, and was recorded at approx. 100.2, Hz in order to extract locomotion velocity.

Visual stimulation. Visual stimuli were presented with Psychtoolbox 3 in MATLAB (Brainard, 1997; Kleiner et al., 2007; Pelli, 1997) to the left eye with a 31.8×56.5 cm (height \times width) monitor (ASUS PB258Q) with a resolution of 1080×1920 pixels positioned 15 cm away from the eye. When the monitor is centered on and perpendicular to the surface of the eye at the closest point, this corresponds to a visual angle of 3.8° at the nearest point and 0.7° at the most remote corner of the monitor. As the craniotomy coverslip placement during surgery and the resulting mouse positioning relative to the objective is optimized for imaging quality and stability, uncontrolled variance in animal

skull position relative to the washer used for head-mounting was compensated with tailored monitor positioning on a six dimensional monitor arm. The pitch of the monitor was kept in the vertical position for all animals, while the roll was visually matched to the roll of the animal's head beneath the headbar by the experimenter. In order to optimize the translational monitor position for centered visual cortex stimulation with respect to the imaging field of view, we used a dot stimulus with a bright background (maximum pixel intensity) and a single dark square dot (minimum pixel intensity). Dot locations were randomly ordered from a 10×10 grid tiling a central square (approx. 90° width and height) with 10 repetitions of 200 ms presentation at each location. The final monitor position for each animal was chosen in order to center the population receptive field of the scan field ROI on the monitor, with the yaw of the monitor visually matched to be perpendicular to and 15 cm from the nearest surface of the eye at that position.

Natural Movies: Natural movies from the “cinematic” and “Sports-1M” (Karpathy et al., 2014) classes were drawn from the library described in (MICrONS Consortium et al., 2021). Each scan contained 360 movies shown one time and 18 movies shown ten times, in both cases drawn equally from the cinematic and Sports-1M classes. Five sets of natural movies were prepared, with each movie unique to its respective set, and each set of movies shown in two scans.

Spatiotemporal Gabors: Spatiotemporal gabor movies were presented as described in (Petkov & Subramanian, 2007; Wang et al., 2023), but with different parameters as described below. For six scans containing spatiotemporal gabors, 72 movies (8 directions \times 3 spatial frequencies \times 3 temporal frequencies) were shown ten times per scan. Gabor spatial frequencies corresponded to wavelengths of 0.05, 0.1, and 0.2 (fraction of monitor width). Gabor temporal frequencies corresponded to gabor velocities of 0.1, 0.2, and 0.3 (fraction of monitor width per second), in the direction perpendicular to the gabor orientation. Gabor spatial envelope was located in the center of the monitor, with a standard deviation of 0.08 (fraction monitor width, approx. 17 degrees). Each gabor movie was 833 ms in duration, and movies were randomly assorted into 6 sequences of 12 conditions each, for a total of 10 seconds per sequence. Because the stimulus was parametrically constructed, the same movies are shown in each of the six scans. Three sets of gabor movies that differ in sequence membership and order were prepared, and each set of movies was shown in two scans.

Directional Pink Noise: Directional pink noise was generated as described in (MICrONS Consortium et al., 2021). For six scans with directional pink noise stimuli, six movie sequences were shown ten times per scan. Each movie sequence was generated from a unique random seed, which determined the underlying pink noise pattern and also the order of 12 equally spaced directional subtrials, with a spatial orientation bias perpendicular to the direction of motion. Each directional subtrial lasted 900 ms, for a

total of 10.8 seconds per sequence. Three sets of directional pink noise movie sequences were prepared, with each sequence unique to its respective set, and each set of sequences shown in two scans.

Random Dot Kinematogram: Random dot kinematograms (RDK) movies were presented as described in (Morrone et al., 2000; Wang et al., 2023), but with different parameters as described below. For six scans containing RDK movies, 32 movies (8 flow trajectories \times 2 velocities \times 2 coherencies) were shown ten times per scan. RDK movie optical flow corresponded to a translational (up/down/left/right), radial (inward / outward w/r/t monitor center), or rotational (clockwise / anticlockwise w/r/t monitor center) trajectory. RDK movie dots had a velocity of either 0.3 or 0.5 (fraction monitor width / second), and coherency of either 50% or 100% with respect to the global optical flow trajectory. Each dot had a diameter of 1/32 (fraction monitor width, approx. 6.7 degrees at the nearest point) and a lifetime of 1 second. Each RDK movie was 2 seconds in duration, and movies were randomly assorted into 8 sequences of 4 movies each, for a total of 8 seconds per sequence. Three sets of RDK movies were prepared, with each movie unique to its respective set, and each set of RDK movies shown in two scans.

Natural Images: Natural image from ImageNet were presented as in (Walker et al., 2019; Wang et al., 2023). For six scans containing natural images, 60 images were shown ten times per scan. Randomly selected images were center-cropped to 9:16 aspect ratio and converted to gray scale. Images were presented for 500 ms, preceded by a 400-600 ms blank gray screen (pixel value 127/255). Images were randomly assorted into 6 sequences of 10 images each, for approx. 10 seconds per sequence. Three sets of natural images were prepared, with each natural image unique to its respective set, and each set of natural images shown in two scans.

Gaussian Dots: Gaussian dots were presented as in (Wang et al., 2023), but with different parameters as detailed below. For six scans containing gaussian dots, 210 dot presentations (105 positions \times 2 dot intensities) were shown ten times per scan. Dot positions were drawn from a grid of 15 horizontal (-0.35 to 0.35) by 7 vertical (-0.267 to 0.267) positions, where all positions are reported as fraction of monitor width and 0 is the center of the monitor. Dots were presented as either white (pixel value 255 out of 255) or black (pixel value 0) on a gray background (pixel value 127). Dot standard deviation was 0.07 (fraction monitor width, $\approx 15^\circ$ at the closest point). Dot presentations were 300 ms in duration, and were randomly assorted into 6 sequences of 35 dots each, for a total of 10.5 seconds per sequence. Because the stimulus was parametrically constructed, the same dots are shown in each of the six scans. Three sets of gaussian dots that differ in sequence membership and order were prepared, and each set of dots was shown in two scans.

A photodiode (TAOS TSL253) was sealed to the top left corner of the monitor, and the voltage was recorded at 10

kHz and timestamped on the behavior clock (MasterClock PCIe-OSC-HSO-2 card). Simultaneous measurement with a luminance meter (LS-100 Konica Minolta) perpendicular to and targeting the center of the monitor was used to generate a lookup table for linear interpolation between photodiode voltage and monitor luminance in cd/m^2 for 16 equidistant values from 0-255, and one baseline value with the monitor unpowered.

At the beginning of each experimental session, we collected photodiode voltage for 52 full-screen pixel values from 0 to 255 for one second trials. The mean photodiode voltage for each trial V_{pd} was fit as a function of the pixel intensity V_{in} :

$$V_{pd} = B + A \times V_{in}^\gamma \quad (2)$$

in order to estimate the γ value of the monitor ($\approx 1.60 - 1.76$). All stimuli were shown with no γ correction.

During the stimulus presentation, sequence information was encoded in a 3 level signal according to the binary encoding of the flip number assigned in-order. This signal underwent a sine convolution, allowing for local peak detection to recover the binary signal. The encoded binary signal was reconstructed for >99% of the flips. A linear fit was applied to the trial timestamps in the behavioral and stimulus clocks, and the offset of that fit was applied to the data to align the two clocks, allowing linear interpolation between them. The mean photodiode voltage of the sequence encoding signal at pixel values 0 and 255 was used to estimate the luminance range of the monitor during the stimulus, with minimum values between 0.001 and 0.65 cd/m^2 and maximum values between 8.7 and 11.3 cd/m^2 in the released scans.

Preprocessing of neural responses and behavioral data.

The full two photon imaging processing pipeline is available at (<https://github.com/cajal/pipeline>). Raster correction for bidirectional scanning phase row misalignment was performed by iterative greedy search at increasing resolution for the raster phase resulting in the maximum cross-correlation between odd and even rows. Motion correction for global tissue movement was performed by shifting each frame in X and Y to maximize the correlation between the cross-power spectra of a single scan frame and a template image, generated from the Gaussian-smoothed average of the Anscombe transform from the middle 2000 frames of the scan. Neurons were automatically segmented using constrained non-negative matrix factorization, then detrended and deconvolved to extract estimates of spiking activity, within the CAIMAN pipeline (Giovannucci et al., 2019). Cells were further selected by a classifier trained to separate somata versus artifacts based on segmented cell masks, resulting in exclusion of 7.1 - 10.1% of masks per scan.

Functional and behavioral signals were resampled to 30 Hz by linear spline interpolation. The mirror motor coordinates of the centroid of each mask was used to assign anatomical coordinates relative to each other and the experimenter's

estimate of the pial surface. Notably, centroid positional coordinates do not carry information about position relative to the area boundaries, or relative to neurons in other scans.

Representation/Core We based our work on the models of [Ecker et al. \(2018\)](#); [Franke et al. \(2022\)](#); [Hoeffling et al. \(2022\)](#); [Lurz et al. \(2021\)](#); [Sinz et al. \(2018\)](#), which are able to predict the responses of a large population of mouse V1 neurons with high accuracy.

For the GRU baseline, we used rotation-equivariant core from [Ecker et al. \(2018\)](#) with 8 rotations, 8 channels, and 4 layers. The spatial kernels were 9×9 , followed by 7×7 . The GRU module, inspired by [Sinz et al. \(2018\)](#), was after the core. It had 64 channels (8 channels \times 8 rotations = 64), and both input and recurrent kernels were 9×9 .

For the 3D Factorized baseline, we used the core inspired by [Hoeffling et al. \(2022\)](#) with 3 layers (32, 64, and 128 channels per layer, resp.). The spatial kernels were 11×11 in the 1st layer and 5×5 in all of the subsequent layers. Similarly, the temporal kernels were 11×1 in the 1st layer and 5×1 afterwards.

The Ensembled baseline cores were same as for the 3D Factorized baseline.

Readout To get the scalar neuronal firing rate for each neuron, we computed a linear regression between the core output tensor of dimensions $\mathbf{x} \in \mathbb{R}^{w \times h \times c}$ (width, height, channels) and the linear weight tensor $\mathbf{w} \in \mathbb{R}^{c \times w \times h}$, followed by an ELU offset by one (ELU+1), to keep the response positive. We made use of the recently proposed Gaussian readout ([Lurz et al., 2021](#)), which simplifies the regression problem considerably. The Gaussian readout learns the parameters of a 2D Gaussian distribution $\mathcal{N}(\mu_n, \Sigma_n)$. The mean μ_n in the readout feature space thus represents the center of a neuron’s receptive field in image space, whereas Σ_n refers to the uncertainty of the receptive field position. During training, a location of height and width in the core output tensor in each training step is sampled, for every image and neuron. Given a large enough initial Σ_n to ensure gradient flow, the uncertainty about the readout location Σ_n is decreasing during training, showing that the estimates of the mean location μ_n becomes more and more reliable. At inference time (i.e. when evaluating our model), we set the readout to be deterministic and to use the fixed position μ_n . In parallel to learning the position, we learned the weights of the weight tensor of the linear regression of size c per neuron. To learn the positions μ_n , we made use of the retinotopic organization of V1 by coupling the recorded cortical 2d-coordinates $\mathbf{p}_n \in \mathbb{R}^2$ of each neuron with the estimation of the receptive field position μ_n of the readout. We achieved this by learning the common function $\mu_n = f(\mathbf{p}_n)$, a randomly initialized linear fully connected MLP of size 2-30-2, shared by all neurons.

Shifter network We employed a free viewing paradigm when presenting the visual stimuli to the head-fixed mice. Thus, the RF positions of the neurons with respect to the presented images had considerable trial-to-trial variability

following any eye movements. We informed our model of the trial dependent shift of neuronal receptive fields due to eye movement by shifting μ_n , the model neuron’s receptive field center, using the estimated eye position (see section Neurophysiological experiments above for details of estimating the pupil center). We passed the estimated pupil center through an MLP (the shifter network), a three layer fully connected network with $n = 5$ hidden features, followed by a *tanh* nonlinearity, that calculates the shift in Δx and Δy of the neurons receptive field in each trial. We then added this shift to the μ_n of each neuron.

Input of behavioral parameters During each presentation of a video, the pupil size and the running speed of the mouse was recorded. We do not have instantaneous pupil dilation change as the target (video) frequency rate is more than the pupil camera sampling frequency. We have used these behavioral parameters to improve the model’s predictivity. Because these behavioral parameters have nonlinear modulatory effects, we decided to append them as separate frames to the input images as new channels ([Franke et al., 2022](#)), such that each new channel simply consisted of the scalar for the respective behavioral parameter recorded in a particular trial, transformed into stimulus dimension. This enabled the model to predict neural responses as a function of both visual input and behavior.

Model training. Both train and validation sets contain only unique videos. We isotropically downsampled all videos to a resolution of 36×64 px ($h \times w$) per frame. Furthermore, we normalized input videos as well as standardized behavioral traces and the target neuronal activities, using the statistics of the training trials of each recording. After this we subsampled 150 subsequent frames randomly from each video and trained our network using the batch size = 8. We used only five competition mice for training, ignoring the pretraining set. A gradient update was performed after 5 batches, 1 per mouse. Then, we trained our networks with the training set by minimizing the Poisson loss $\frac{1}{m} \sum_{i=1}^m (\hat{r}^{(i)} - r^{(i)} \log \hat{r}^{(i)})$, where m denotes the number of neurons, \hat{r} the predicted neuronal response and r the observed response. For Poisson loss each frame was treated independently, and no time component was included. After each epoch, i.e. full pass through the training set, we calculated the correlation between predicted and measured neuronal responses on the validation set and averaged it across all neurons. If the correlation failed to increase for five consecutive epochs, we stopped the training and restored the model to its state after the best performing epoch. Then, we either decreased the learning rate by a factor of 0.3 or stopped training altogether, if the number of learning-rate decay steps was reached (n=4 decay steps). We optimized the network’s parameters using the Adam optimizer ([Kingma & Ba, 2015](#)). All parameters and hyper-parameters regarding model architecture and training procedure can be found in our `sensorium` repository (see Code Availability).

Metrics. We chose correlation to evaluate the models performance.

Since **correlation** is invariant to shift and scale of the predictions, it does not reward a correct prediction of the absolute value of the neural response but rather the neuron's relative response changes. It is bound to $[-1, 1]$ and thus easily interpretable. However, without accounting for the unexplainable noise in neural responses, the upper bound of 1 cannot be reached, which can be misleading.

Single Trial Correlation To evaluate model performance on variation between individual trials, we will compute correlation ρ_{st} between predicted single-trial activity o_{ij} and single-trial neuronal responses r_{ij} , as

$$\rho_{st} = \text{corr}(\mathbf{r}_{st}, \mathbf{o}_{st}) = \frac{\sum_{i,j} (r_{ij} - \bar{r})(o_{ij} - \bar{o})}{\sqrt{\sum_{i,j} (r_{ij} - \bar{r})^2 \sum_{i,j} (o_{ij} - \bar{o})^2}}, \quad (3)$$

where r_{ij} is the i -th frame of j -th video repeat, o_{ij} is the corresponding prediction, \bar{r} is the average response to all the videos in the test subset across all repeats, and \bar{o} is the average prediction for all the videos in the test subset across all repeats. ρ_{st} is computed independently per neuron and then averaged across all neurons to produce the final metric.

Correlation to Average We calculate the *correlation to average* ρ_{ta} in a similar way to the single-trial correlation, but we first average the responses and predictions per frame across all video repeats before computing.

$$\rho_{ta} = \text{corr}(\mathbf{r}_{ta}, \mathbf{o}_{ta}) = \frac{\sum_{i,j} (\bar{r}_i - \bar{r})(\bar{o}_i - \bar{o})}{\sqrt{\sum_i (\bar{r}_i - \bar{r})^2 \sum_i (\bar{o}_i - \bar{o})^2}}, \quad (4)$$

where \bar{r}_i is a response averaged over stimulus repeats for a fixed neuron.

Code and data availability. Our competition website can be reached under <https://www.sensorium-competition.net/>. The pretraining dataset split is available for download via DeepLake (Hambarzumyan et al., 2022) upon the competition start, under license CC BY-NC-ND 4.0. Our coding framework uses general tools including PyTorch, Numpy, scikit-image, matplotlib, seaborn, DataJoint, Jupyter, Docker, CAIMAN, DeepLabCut, Psychtoolbox, Scanimage, and Kubernetes. We also used the following custom libraries and code: `neuralpredictors` (<https://github.com/sinzlab/neuralpredictors>) for torch-based custom functions for model implementation and `sensorium` for utilities (https://github.com/ecker-lab/sensorium_2023).

References

Adelson, E. H., & Bergen, J. R. (1985). Spatiotemporal energy models for the perception of motion. *J. Opt. Soc. Am.*, 2(2), 284–299.

Allen-Zhu, Z., & Li, Y. (2023). Towards understanding ensemble, knowledge distillation and self-distillation in deep learning. *arXiv*.

Antolík, J., Hofer, S. B., Bednar, J. A., & Mrcic-Flogel, T. D. (2016). Model constrained by visual hierarchy improves prediction of neural responses to natural scenes. *PLoS Comput. Biol.*, (pp. 1–22).

Bashiri, M., Walker, E., Lurz, K.-K., Jagadish, A., Muhammad, T., Ding, Z., Ding, Z., Tolia, A., & Sinz, F. (2021). A flow-based latent state generative model of neural population responses to natural images. *Adv. Neural Inf. Process. Syst.*, 34.

Bashivan, P., Kar, K., & DiCarlo, J. J. (2019). Neural population control via deep image synthesis. *Science (New York, N.Y.)*, 364(6439).

Batty, E., Merel, J., Brackbill, N., Heitman, A., Sher, A., Litke, A., Chichilnisky, E., & Paninski, L. (2017). Multilayer recurrent network models of primate retinal ganglion cell responses. In *International Conference on Learning Representations*.

Brainard, D. H. (1997). The psychophysics toolbox. *Spat. Vis.*, 10(4), 433–436.

Burg, M. F., Cadena, S. A., Denfield, G. H., Walker, E. Y., Tolia, A. S., Bethge, M., & Ecker, A. S. (2021). Learning divisive normalization in primary visual cortex. *PLOS Computational Biology*, 17(6), e1009028.

Cadena, S. A., Denfield, G. H., Walker, E. Y., Gatsys, L. A., Tolia, A. S., Bethge, M., & Ecker, A. S. (2019). Deep convolutional models improve predictions of macaque v1 responses to natural images. *PLOS Computational Biology*, 15(4), e1006897.

Cadiou, C. F., Hong, H., Yamins, D. L. K., Pinto, N., Ardila, D., Solomon, E. A., Majaj, N. J., & DiCarlo, J. J. (2014). Deep neural networks rival the representation of primate IT cortex for core visual object recognition. *PLoS Comput. Biol.*, 10(12), e1003963.

Cichy, R. M., Dwivedi, K., Lahner, B., Lascelles, A., Iamshchinina, P., Graumann, M., Andonian, A., Murty, N. A. R., Kay, K., Roig, G., & Oliva, A. (2021). The algonauts project 2021 challenge: How the human brain makes sense of a world in motion. *arXiv*.

Cichy, R. M., Roig, G., Andonian, A., Dwivedi, K., Lahner, B., Lascelles, A., Mohsenzadeh, Y., Ramakrishnan, K., & Oliva, A. (2019). The algonauts project: A platform for communication between the sciences of biological and artificial intelligence. *arXiv*.

Cowley, B., & Pillow, J. (2020). High-contrast “gaudy” images improve the training of deep neural network models of visual cortex. In H. Larochelle, M. Ranzato, R. Hadsell, M. Balcan, & H. Lin (Eds.) *Advances in Neural Information Processing Systems 33*, (pp. 21591–21603). Curran Associates, Inc.

de Vries, S. E. J., Lecoq, J. A., Buice, M. A., Groblewski, P. A., Ocker, G. K., Oliver, M., Feng, D., Cain, N., Ledochowitsch, P., Millman, D., Roll, K., Garrett, M., Keenan, T., Kuan, L., Mihalas, S., Olsen, S., Thompson, C., Wakeman, W., Waters, J., Williams, D., Barber, C., Beresque, N., Blanchard, B., Bowles, N., Caldejon, S. D., Casal, L., Cho, A., Cross, S., Dang, C., Dolbeare, T., Edwards, M., Galbraith, J., Gaudreault, N., Gilbert, T. L., Griffin, F., Hargrave, P., Howard, R., Huang, L., Jewell, S., Keller, N., Knoblich, U., Larkin, J. D., Larsen, R., Lau, C., Lee, E., Lee, F., Leon, A., Li, L., Long, F., Luviano, J., Mace, K., Nguyen, T., Perkins, J., Robertson, M., Seid, S., Shea-Brown, E., Shi, J., Sjoquist, N., Slaughterbeck, C., Sullivan, D., Valenza, R., White, C., Williford, A., Witten, D. M., Zhuang, J., Zeng, H., Farrell, C., Ng, L., Bernard, A., Phillips, J. W., Reid, R. C., & Koch, C. (2020). A large-scale standardized physiological survey reveals functional organization of the mouse visual cortex. *Nat. Neurosci.*, 23(1), 138–151.

Dean, J., Patterson, D., & Young, C. (2018). A new golden age in computer architecture: Empowering the machine-learning revolution. *IEEE Micro*, 38(2), 21–29.

Ding, Z., Fahey, P. G., Papadopoulos, S., Wang, E., Celli, B., Papadopoulos, C., Kunin, A., Chang, A., Fu, J., Ding, Z., Patel, S., Ponder, K., Alexander Bae, J., Bodor, A. L., Brittain, D., Buchanan, J., Bumbarger, D. J., Castro, M. A., Cobos, E., Dorkenwald, S., Elabbady, L., Halageri, A., Jia, Z., Jordan, C., Kapner, D., Kemnitz, N., Kinn, S., Lee, K., Li, K., Lu, R., Macrina, T., Mahalingam, G., Mitchell, E., Mondal, S. S., Mu, S., Nehoran, B., Popovych, S., Schneider-Mizell, C. M., Silversmith, W., Takeno, M., Torres, R., Turner, N. L., Wong, W., Wu, J., Yin, W., Yu, S.-C., Froudarakis, E., Sinz, F. H., Sebastian Seung, H., Collman, F., da Costa, N. M., Clay Reid, R., Walker, E. Y., Pitkow, X., Reimer, J., & Tolia, A. S. (2023a). Functional connectomics reveals general wiring rule in mouse visual cortex. *bioRxiv*, (p. 2023.03.13.531369).

Ding, Z., Tran, D. T., Ponder, K., Cobos, E., Ding, Z., Fahey, P. G., Wang, E., Muhammad, T., Fu, J., Cadena, S. A., et al. (2023b). Bipartite invariance in mouse primary visual cortex. *bioRxiv*. URL <https://www.biorxiv.org/content/10.1101/2023.03.15.532836v1>

Ecker, A. S., Sinz, F. H., Froudarakis, E., Fahey, P. G., Cadena, S. A., Walker, E. Y., Cobos, E., Reimer, J., Tolia, A. S., & Bethge, M. (2018). A rotation-equivariant convolutional neural network model of primary visual cortex. *arXiv*.

Franke, K., Willeke, K. F., Ponder, K., Galdamez, M., Zhou, N., Muhammad, T., Patel, S., Froudarakis, E., Reimer, J., Sinz, F. H., & Tolia, A. S. (2022). State-dependent pupil dilation rapidly shifts visual feature selectivity. *Nature*, 610(7930), 128–134. URL <https://doi.org/10.1038/s41586-022-05270-3>

Froudarakis, E., Berens, P., Ecker, A. S., Cotton, R. J., Sinz, F. H., Yatsenko, D., Saggau, P., Bethge, M., & Tolia, A. S. (2014). Population code in mouse V1 facilitates readout of natural scenes through increased sparseness. *Nat. Neurosci.*, 17(6), 851–857.

Fu, J., Shrinivasan, S., Ponder, K., Muhammad, T., Ding, Z., Wang, E., Ding, Z., Tran, D. T., Fahey, P. G., Papadopoulos, S., Patel, S., Reimer, J., Ecker, A. S., Pitkow, X., Haefner, R. M., Sinz, F. H., Franke, K., & Tolia, A. S. (2023). Pattern completion and disruption characterize contextual modulation in mouse visual cortex. *bioRxiv*. URL <https://www.biorxiv.org/content/early/2023/03/14/2023.03.13.532473>

Garrett, M. E., Nauhaus, I., Marshel, J. H., & Callaway, E. M. (2014). Topography and areal organization of mouse visual cortex. *J. Neurosci.*, 34(37), 12587–12600.

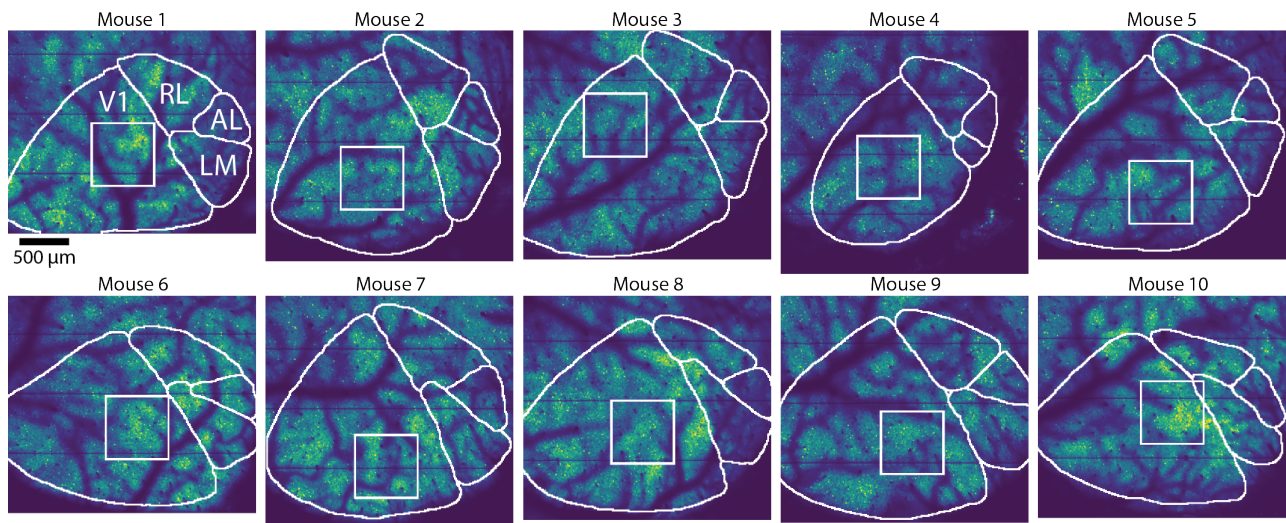
George, D., & Hawkins, J. (2005). A hierarchical bayesian model of invariant pattern recognition in the visual cortex. In *Proceedings. 2005 IEEE International Joint Conference on Neural Networks, 2005*, vol. 3, (pp. 1812–1817). IEEE.

Gifford, A. T., Lahner, B., Saba-Sadiya, S., Vilas, M. G., Lascelles, A., Oliva, A., Kay, K., Roig, G., & Cichy, R. M. (2023). The algonauts project 2023 challenge: How the human brain makes sense of natural scenes. *arXiv preprint arXiv:2301.03198*.

Giovannucci, A., Friedrich, J., Gunn, P., Kalfon, J., Brown, B. L., Koay, S. A., Taxis, J., Najafi, F., Gauthier, J. L., Zhou, P., Khakh, B. S., Tank, D. W., Chklovskii, D. B., & Pnevmatikakis, E. A. (2019). CalmAn: An open source tool for scalable calcium imaging data analysis. *Elife*, 8, e38173.

Haefner, R., & Cumming, B. (2008). An improved estimator of variance explained in the presence of noise. In D. Koller, D. Schuurmans, Y. Bengio, & L. Bottou (Eds.) *Advances in Neural*

- Information Processing Systems, vol. 21. Curran Associates, Inc.
URL <https://proceedings.neurips.cc/paper/2008/file/2ab56412b1163ee131e1246da0955bd1-Paper.pdf>
- Hambardzumyan, S., Tuli, A., Ghukasyan, L., Rahman, F., Topchyan, H., Isayan, D., McQuade, M., Harutyunyan, M., Hakobyan, T., Stranic, I., & Buniatyun, D. (2022). Deep lake: a lakehouse for deep learning. *arXiv*.
- Heeger, D. J. (1992a). Half-squaring in responses of cat striate cells. *Vis. Neurosci.*, *9*(5), 427–443.
- Heeger, D. J. (1992b). Normalization of cell responses in cat striate cortex. *Vis. Neurosci.*, *9*(2), 181–197.
- Hoefling, L., Szatko, K. P., Behrens, C., Qiu, Y., Klindt, D. A., Jessen, Z., Schwartz, G. S., Bethge, M., Berens, P., Franke, K., et al. (2022). A chromatic feature detector in the retina signals visual context changes. *bioRxiv*, (pp. 2022–11).
URL <https://www.biorxiv.org/content/10.1101/2022.11.30.518492.abstract>
- Hsu, A., Borst, A., & Theunissen, F. E. (2004). Quantifying variability in neural responses and its application for the validation of model predictions. *Network: Computation in Neural Systems*, *15*(2), 91–109.
- Jones, J. P., & Palmer, L. A. (1987). The two-dimensional spatial structure of simple receptive fields in cat striate cortex. *J. Neurophysiol.*, *58*(6), 1187–1211.
- Karpathy, A., Toderici, G., Shetty, S., Leung, T., Sukthakar, R., & Fei-Fei, L. (2014). Large-Scale video classification with convolutional neural networks. In *2014 IEEE Conference on Computer Vision and Pattern Recognition*, (pp. 1725–1732).
- Kindel, W. F., Christensen, E. D., & Zylberberg, J. (2019). Using deep learning to probe the neural code for images in primary visual cortex. *Journal of vision*, *19*(4), 29–29.
- Kingma, D. P., & Ba, J. (2015). Adam: A method for stochastic optimization. In Y. Bengio, & Y. LeCun (Eds.), *3rd International Conference on Learning Representations, ICLR 2015, San Diego, CA, USA, May 7-9, 2015, Conference Track Proceedings*.
- Kleiner, M. B., Brainard, D. H., Pelli, D. G., Ingling, A., & Broussard, C. (2007). What's new in psychtoolbox-3. *Perception*, *36*, 1–16.
- Klindt, D. A., Ecker, A. S., Euler, T., & Bethge, M. (2017). Neural system identification for large populations separating “what” and “where”. In *Advances in Neural Information Processing Systems*, (pp. 4–6).
- Li, B. M., Cornacchia, I. M., Rochefort, N. L., & Onken, A. (2023). V1t: large-scale mouse v1 response prediction using a vision transformer. *arXiv*.
- Liu, J. K., Schreyer, H. M., Onken, A., Rozenblit, F., Khani, M. H., Krishnamoorthy, V., Panzeri, S., & Gollisch, T. (2017). Inference of neuronal functional circuitry with spike-triggered non-negative matrix factorization. *Nature communications*, *8*(1), 149.
- Lurz, K.-K., Bashiri, M., Willeke, K., Jagadish, A. K., Wang, E., Walker, E. Y., Cadena, S. A., Muhammad, T., Cobos, E., Tolia, A. S., Ecker, A. S., & Sinz, F. H. (2021). Generalization in data-driven models of primary visual cortex. In *Proceedings of the International Conference for Learning Representations (ICLR)*, (p. 2020.10.05.326256).
- Marques, T., Nguyen, J., Fioreze, G., & Petreanu, L. (2018). The functional organization of cortical feedback inputs to primary visual cortex. *Nature neuroscience*, *21*(5), 757–764.
- Mathis, A., Mamidanna, P., Cury, K. M., Abe, T., Murthy, V. N., Mathis, M. W., & Bethge, M. (2018). DeepLabCut: markerless pose estimation of user-defined body parts with deep learning. *Nat. Neurosci.*, *21*(9), 1281–1289.
- McIntosh, L. T., Maheswaranathan, N., Nayebi, A., Ganguli, S., & Baccus, S. A. (2016). Deep learning models of the retinal response to natural scenes. *Adv. Neural Inf. Process. Syst.*, *29*(Nips), 1369–1377.
- MICrONS Consortium, Alexander Bae, J., Baptiste, M., Bodor, A. L., Brittain, D., Buchanan, J., Bumbarger, D. J., Castro, M. A., Celii, B., Cobos, E., Collman, F., da Costa, N. M., Dorkenwald, S., Elabbady, L., Fahey, P. G., Filis, T., Froudakis, E., Gager, J., Gamlin, C., Halageri, A., Hebditch, J., Jia, Z., Jordan, C., Kapner, D., Kemnitz, N., Kinn, S., Koolman, S., Kuehner, K., Lee, K., Li, K., Lu, R., Macrina, T., Mahalingam, G., McReynolds, S., Miranda, E., Mitchell, E., Mondal, S. S., Moore, M., Mu, S., Muhammad, T., Nehoran, B., Ogedengbe, O., Papadopoulos, C., Papadopoulos, S., Patel, S., Pitkow, X., Popovich, S., Ramos, A., Clay Reid, R., Reimer, J., Schneider-Mizell, C. M., Sebastian Seung, H., Silverman, B., Silversmith, W., Sterling, A., Sinz, F. H., Smith, C. L., Suckow, S., Tan, Z. H., Tolia, A. S., Torres, R., Turner, N. L., Walker, E. Y., Wang, T., Williams, G., Williams, S., Willie, K., Willie, R., Wong, W., Wu, J., Xu, C., Yang, R., Yatsenko, D., Ye, F., Yin, W., & Yu, S.-C. (2021). Functional connectomics spanning multiple areas of mouse visual cortex. *bioRxiv*, (p. 2021.07.28.454025).
- Morrone, M. C., Tosetti, M., Montanaro, D., Fiorentini, A., Cioni, G., & Burr, D. C. (2000). A cortical area that responds specifically to optic flow, revealed by fMRI. *Nat. Neurosci.*, *3*(12), 1322–1328.
- Niell, C. M., & Stryker, M. P. (2010). Modulation of visual responses by behavioral state in mouse visual cortex. *Neuron*, *65*(4), 472–479.
- Pasupathy, A., & Connor, C. E. (2001). Shape representation in area v4: position-specific tuning for boundary conformation. *Journal of neurophysiology*.
- Pei, F., Ye, J., Zoltowski, D., Wu, A., Chowdhury, R. H., Sohn, H., O'Doherty, J. E., Shenoy, K. V., Kaufman, M. T., Churchland, M., et al. (2021). Neural latents benchmark'21: evaluating latent variable models of neural population activity. *arXiv preprint arXiv:2109.04463*.
- Pelli, D. G. (1997). The VideoToolbox software for visual psychophysics: transforming numbers into movies. *Spat. Vis.*, *10*(4), 437–442.
- Perrone, J. A., & Liston, D. B. (2015). Redundancy reduction explains the expansion of visual direction space around the cardinal axes. *Vision Research*, *111*, 31–42.
- Petkov, N., & Subramanian, E. (2007). Motion detection, noise reduction, texture suppression, and contour enhancement by spatiotemporal gabor filters with surround inhibition. *Biol. Cybern.*, *97*(5-6), 423–439.
- Ponce, C. R., Xiao, W., Schade, P. F., Hartmann, T. S., Kreiman, G., & Livingstone, M. S. (2019). Evolving images for visual neurons using a deep generative network reveals coding principles and neuronal preferences. *Cell*, *177*(4), 999–1009.e10.
- Pospisil, D. A., & Bair, W. (2020). The unbiased estimation of the fraction of variance explained by a model.
- Reimer, J., Froudarakis, E., Cadwell, C. R., Yatsenko, D., Denfield, G. H., & Tolia, A. S. (2014). Pupil fluctuations track fast switching of cortical states during quiet wakefulness. *Neuron*, *84*(2), 355–362.
- Ren, Y., & Bashivan, P. (2023). How well do models of visual cortex generalize to out of distribution samples? *bioRxiv*, (pp. 2023–05).
- Roddey, J. C., Girish, B., & Miller, J. P. (2000). Assessing the performance of neural encoding models in the presence of noise. *Journal of computational neuroscience*, *8*, 95–112.
- Russakovsky, O., Deng, J., Su, H., Krause, J., Satheesh, S., Ma, S., Huang, Z., Karpathy, A., Khosla, A., Bernstein, M., Berg, A. C., & Fei-Fei, L. (2015). ImageNet large scale visual recognition challenge. *Int. J. Comput. Vis.*, *115*(3), 211–252.
- Rust, N. C., Schwartz, O., Movshon, J. A., & Simoncelli, E. P. (2005). Spatiotemporal elements of macaque v1 receptive fields. *Neuron*, *46*(6), 945–956.
- Schoppe, O., Harper, N. S., Willmore, B. D. B., King, A. J., & Schnupp, J. W. H. (2016). Measuring the performance of neural models. *Frontiers in Computational Neuroscience*, *10*.
URL <https://doi.org/10.3389/fncom.2016.00010>
- Schrimpf, M., Kubilius, J., Hong, H., Majaj, N. J., Rajalingham, R., Issa, E. B., Kar, K., Bashivan, P., Prescott-Roy, J., Geiger, F., et al. (2018). Brain-score: Which artificial neural network for object recognition is most brain-like? *bioRxiv*, (p. 407007).
- Schrimpf, M., Kubilius, J., Lee, M. J., Ratan Murty, N. A., Ajemian, R., & DiCarlo, J. J. (2020). Integrative benchmarking to advance neurally mechanistic models of human intelligence. *Neuron*, *108*(3), 413–423.
- Siegle, J. H., Jia, X., Durand, S., Gale, S., Bennett, C., Graddis, N., Heller, G., Ramirez, T. K., Choi, H., Luviano, J. A., Groblewski, P. A., Ahmed, R., Arkhipov, A., Bernard, A., Billeh, Y. N., Brown, D., Buice, M. A., Cain, N., Caldejon, S., Casal, L., Cho, A., Chvilicek, M., Cox, T. C., Dai, K., Denman, D. J., de Vries, S. E. J., Dietzman, R., Esposito, L., Farrell, C., Feng, D., Galbraith, J., Garrett, M., Gelfand, E. C., Hancock, N., Harris, J. A., Howard, R., Hu, B., Hytner, R., Iyer, R., Jessett, E., Johnson, K., Kato, I., Kiggins, J., Lambert, S., Lecoq, J., Ledochowitsch, P., Lee, J. H., Leon, A., Li, Y., Liang, E., Long, F., Mace, K., Melchior, J., Millman, D., Mollenkopf, T., Nayan, C., Ng, L., Ngo, K., Nguyen, T., Nicovich, P. R., North, K., Ocker, G. K., Ollerenshaw, D., Oliver, M., Pachitariu, M., Perkins, J., Reding, M., Reid, D., Robertson, M., Ronellenfitch, K., Seid, S., Slaughterbeck, C., Stoecklin, M., Sullivan, D., Sutton, B., Swapp, J., Thompson, C., Turner, K., Wakeman, W., Whitesell, J. D., Williams, D., Williford, A., Young, R., Zeng, H., Naylor, S., Phillips, J. W., Reid, R. C., Mihalas, S., Olsen, S. R., & Koch, C. (2021). Survey of spiking in the mouse visual system reveals functional hierarchy. *Nature*, *592*(7852), 86–92.
- Simoncelli, E. P., Paninski, L., Pillow, J., Schwartz, O., et al. (2004). Characterization of neural responses with stochastic stimuli. *The cognitive neurosciences*, *3*(327-338), 1.
- Sinz, F., Ecker, A. S., Fahey, P., Walker, E., Cobos, E., Froudarakis, E., Yatsenko, D., Pitkow, Z., Reimer, J., & Tolia, A. (2018). Stimulus domain transfer in recurrent models for large scale cortical population prediction on video. *Advances in neural information processing systems*, *31*.
- Sofroniew, N. J., Flickinger, D., King, J., & Svoboda, K. (2016). A large field of view two-photon microscope with subcellular resolution for in vivo imaging. *elife*, *5*, e14472.
- Touryan, J., Felsen, G., & Dan, Y. (2005). Spatial structure of complex cell receptive fields measured with natural images. *Neuron*, *45*(5), 781–791.
- Ustyuzhaninov, I., Burg, M. F., Cadena, S. A., Fu, J., Muhammad, T., Ponder, K., Froudarakis, E., Ding, Z., Bethge, M., Tolia, A. S., et al. (2022). Digital twin reveals combinatorial code of non-linear computations in the mouse primary visual cortex. *bioRxiv*, (pp. 2022–02).
- Vintch, B., Movshon, J. A., & Simoncelli, E. P. (2015). A convolutional subunit model for neuronal responses in macaque v1. *Journal of Neuroscience*, *35*(44), 14829–14841.
- Walker, E. Y., Cotton, R. J., Ma, W. J., & Tolia, A. S. (2020). A neural basis of probabilistic computation in visual cortex. *Nature Neuroscience*, *23*(1), 122–129.
- Walker, E. Y., Sinz, F. H., Cobos, E., Muhammad, T., Froudarakis, E., Fahey, P. G., Ecker, A. S., Reimer, J., Pitkow, X., & Tolia, A. S. (2019). Inception loops discover what excites neurons most using deep predictive models. *Nat. Neurosci.*, *22*(12), 2060–2065.
- Wang, E. Y., Fahey, P. G., Ponder, K., Ding, Z., Chang, A., Muhammad, T., Patel, S., Ding, Z., Tran, D., Fu, J., Papadopoulos, S., Franke, K., Ecker, A. S., Reimer, J., Pitkow, X., Sinz, F. H., & Tolia, A. S. (2023). Towards a foundation model of the mouse visual cortex. *bioRxiv*.
URL <https://www.biorxiv.org/content/early/2023/03/24/2023.03.21.533548>
- Willeke, K. F., Fahey, P. G., Bashiri, M., Pedo, L., Burg, M. F., Blessing, C., Cadena, S. A., Ding, Z., Lurz, K.-K., Ponder, K., Muhammad, T., Patel, S. S., Ecker, A. S., Tolia, A. S., & Sinz, F. H. (2022). The sensorium competition on predicting large-scale mouse primary visual cortex activity.
URL <https://arxiv.org/abs/2206.08666>
- Yamins, D. L. K., Hong, H., Cadieu, C. F., Solomon, E. A., Seibert, D., & DiCarlo, J. J. (2014). Performance-optimized hierarchical models predict neural responses in higher visual cortex. *Proceedings of the National Academy of Sciences*, *111*(23), 8619–8624.
URL <https://doi.org/10.1073/pnas.1403112111>
- Zhang, Y., Lee, T.-S. T. S., Li, M., Liu, F., Tang, S., Sing, T., Ming, L., Fang, L., Shimming, L., Lee, T.-S. T. S., Li, M., Liu, F., & Tang, S. (2018). Convolutional neural network models of V1 responses to complex patterns. *J. Comput. Neurosci.*, (pp. 1–22).
- Zheng, Y., Jia, S., Yu, Z., Liu, J. K., & Huang, T. (2021). Unraveling neural coding of dynamic natural visual scenes via convolutional recurrent neural networks. *Patterns*, *2*(10), 100350.



Supplemental Fig. 1. Scan field locations within primary visual cortex. Registered location of the scan field (white rectangle) to retinotopic mapping scan with manually annotated area boundaries (white lines) for primary visual cortex (V1) and anterolateral (AL), rostralateral (RL), and lateromedial (LM) higher visual areas.